Investigation of the ^{244}Pu(^{48}Ca,xn)$^{292-x}$Fl reaction with the LBNL SHREC detector: Investigation of decay chains of isotopes of flerovium (Z = 114)

Gates, J. M.; Orford, R.; Rudolph, D.; Chemey, A. T.; Clark, Roderick M.; Crawford, H. L.; Fallon, P.; Folden, C. M.; Garcia, F. H.; Golubev, P.; Gooding, J.A. ; Gregorich, K. E.; Henderson, R. A.; Hrabar, Y.; Kirkland, A. S.; McCarthy, M.; Mildon, J. A.; Pore, J. L.; Porzio, C.; Rice, E.; Sarmiento, L. G.; Stoyer, M. A.; Thomas, K.; Wooddy, P. T.

Published in:
Physical Review C

DOI:
10.1103/kjyy-t1nk

2026

Document Version:
Publisher's PDF, also known as Version of record

Investigation of the ^{244}Pu(^{48}Ca, xn)$^{292-x}$Fl reaction with the LBNL SHREC detector: Investigation of decay chains of isotopes of flerovium ($Z = 114$)

J. M. Gates,[1,*] R. Orford,[1] D. Rudolph,[2,1] A. T. Chemey,[3] R. M. Clark,[1] H. L. Crawford,[1] P. Fallon,[1] C. M. Folden, III,[4,5] F. H. Garcia,[1,†] P. Golubev,[2,1] J. A. Gooding,[1,6] K. E. Gregorich,[7] R. A. Henderson,[7] Y. Hrabar,[2] A. S. Kirkland,[4,5] M. McCarthy,[1,6] J. A. Mildon,[4,5] J. L. Pore,[1] C. Porzio,[1,‡] E. Rice,[1,6] L. G. Sarmiento,[2] M. A. Stoyer,[7,1] K. Thomas,[7] and P. T. Wooddy[7]

[1]*Nuclear Science Division, Lawrence Berkeley National Laboratory, Berkeley, California 94720, USA*
[2]*Department of Physics, Lund University, 22100 Lund, Sweden*
[3]*Department of Nuclear Science and Engineering, Oregon State University, Corvallis, Oregon 97331, USA*
[4]*Cyclotron Institute, Texas A&M University, College Station, Texas 77843, USA*
[5]*Department of Chemistry, Texas A&M University, College Station, Texas 77843, USA*
[6]*Department of Nuclear Engineering, University of California, Berkeley, California 94720, USA*
[7]*Physical and Life Sciences Directorate, Lawrence Livermore National Laboratory, Livermore, California 94550, USA*

(Received 3 September 2025; accepted 1 December 2025; published 13 February 2026)

The ^{244}Pu(^{48}Ca, xn)$^{292-x}$Fl reaction was investigated at Lawrence Berkeley National Laboratory's 88 Inch Cyclotron using the Berkeley Gas-filled Separator (BGS), the newly installed Superheavy Recoil detector, along with an upgraded digital electronics and data acquisition system. Seven decay chains were observed starting with an evaporation residue, followed by a single α decay and a spontaneous fission. The decay characteristics of these seven decay chains led to an assignment to ^{288}Fl, the product of the 4n reaction channel. Two additional chains were (tentatively) assigned to the decay of the 3n exit channel, ^{289}Fl. Cross sections for the 4n and 3n exit channels were $\sigma_{\text{prod}} = 6.7(^{36}_{25})$ pb and $\sigma_{\text{prod}} = 1.6(^{22}_{11})$ pb, respectively. Another decay chain, tentatively assigned to the 5n exit channel through the ^{48}Ca + ^{244}Pu reaction or the 3n exit channel of the ^{48}Ca + ^{242}Pu reaction, was also detected. Detailed information regarding the observed decay chains and their nuclear structure aspects is discussed, along with the performance of the BGS and the new detection system.

DOI: 10.1103/kjyy-t1nk

I. INTRODUCTION

The production of superheavy elements (SHEs, $Z \geqslant 104$) and the exploration of their nuclear properties represent a significant frontier in modern nuclear physics, offering deeper insights into the fundamental building blocks of matter. These elements owe their existence to nuclear shell effects, which provide enhanced stability to otherwise highly unstable systems. Without the stabilizing influence of these shells, SHEs are predicted to decay in less than 10^{-14} seconds—shorter than the time required for an electron shell to form around the nucleus, which defines the existence of an element [1].

The production of technetium in 1937 marked the first discovery of an element that is not naturally occurring on Earth [2]. Since then, 30 elements have been added to the periodic table of the elements—two of which occur naturally on Earth. This is an average of one new element every three years for the last 90 years! To date, scientists around the world have discovered elements up to oganesson, with $Z = 118$ [3].

All currently known SHEs have been discovered in compound-nucleus fusion-evaporation reactions. Here, the nuclei of two lighter elements are fused together into a compound nucleus that is formed in an excited state. SHEs are formed when that compound nucleus deexcites through the emission of neutrons and γ rays, instead of fission. As of today, all known SHE isotopes with $Z = 104-118$ have been produced using only one of three different types of nuclear reactions. Elements with $Z = 101-106$ were first made by impinging light-ion beams (e.g., N, O, F, Ne, or Si) on actinide targets. The resulting highly excited compound nucleus would then deexcite through the emission of 4–6 neutrons in so-called "hot-fusion" reactions [4]. Elements with $Z = 107-113$ were discovered by combining transition metal beams (e.g., ^{50}Ti, ^{51}V, ^{54}Cr, ^{62,64}Ni, or ^{70}Zn) with targets of Pb or Bi. These reactions led to much lower excitation energies of the compound nucleus, which would deexcite through the emission of only one or two neutrons in so-called "cold-fusion" reactions. Unfortunately, both of these reactions show similar properties: the production rate drops by up to an order of magnitude with each unit increase in Z of the compound nucleus.

After copernecium ($Z = 112$) was discovered in 1996 [5], the future of new element searches was looking bleak: without a new reaction, these rapidly decreasing cross sections looked

*Contact author: jmgates@lbl.gov
†Present address: Department of Chemistry, Simon Fraser University, Burnaby, British Columbia V5A 1S6, Canada.
‡Present address: CERN-ISOLDE, 1211 Geneva 23, Switzerland.

to spell the end to element discovery with the current generation of low-energy, heavy-ion beam accelerators by $Z = 113$ or $Z = 114$. Luckily, a major breakthrough in SHE research was underway at the Joint Institute for Nuclear Research (JINR) in Dubna, Russia, where they were bombarding actinide targets with doubly magic ^{48}Ca [3]. In just a few years, the new elements flerovium, moscovium, livermorium, tennessine, and oganesson ($Z = 114-118$) were discovered [6,7]. What sets this reaction apart is the surprisingly high production cross sections, estimated to be orders of magnitude higher than that expected from hot- or cold-fusion reactions. For example, when nihonium ($Z = 113$) became the heaviest element produced via a cold fusion reaction, only three atoms were observed during over 500 days of irradiating a ^{209}Bi target with a beam of ^{70}Zn [8,9] leading to a cross section of $22(^{20}_{13})$fb. By contrast, more neutron-rich isotopes of the same element were produced using the $^{48}\mathrm{Ca} + ^{237}\mathrm{Np}$ reaction at a cross section of $0.9(^{1.6}_{0.6})$pb, or nearly 40 times higher production rates [10].

Furthermore, interesting effects were observed with the ^{48}Ca reactions on actinides: the production cross sections increase as Z is increased from $Z = 112$ through $Z = 115$, before again beginning to decrease with increased proton number beyond $Z = 115$. Additionally, the more than 50 new isotopes produced in these reactions are all more neutron rich than those produced in hot- or cold-fusion reactions. For a given element, this leads to longer lifetimes of the nuclei. With these discoveries, it is conjectured that we are beginning to reach the shores of the "island of stability" [11], a region of the nuclear landscape where predictions since the 1950s have suggested there may be relatively long-lived far-transuranic nuclei [11–16].

At present, we have seemingly once again reached the limit of element discovery with ^{48}Ca beams with oganesson ($Z = 118$). While cross sections for the production of elements 119 or 120 with ^{48}Ca beams on Es or Fm targets should have sufficiently high production rates to observe elements 119 and 120 at today's facilities, Es and Fm are not available in suitable quantities to make targets for irradiation, even though "only" a few tens of milligrams of material are required.

New reactions or reaction mechanisms are once again needed to move toward discovering new elements. Multiple theoretical studies have coalesced on the conclusion that the solution for producing new elements lies in switching to irradiating actinide targets with beams heavier than ^{48}Ca, such as ^{50}Ti, ^{51}V, or ^{54}Cr [17–35]. However, experimental attempts to make new elements with $Z = 119$, 120, and 122 [36–39] have been unsuccessful as of today. Recently, though, new results have shown that the SHE livermorium ($Z = 116$) can be produced with either ^{50}Ti [40,41] or ^{54}Cr beams [41], albeit with a decrease in cross sections of approximately one or two orders of magnitude for ^{50}Ti or ^{54}Cr, respectively, as compared with ^{48}Ca beams.

While we could soon be moving into a new era of element discovery following tennessine's discovery in 2010, there will likely be new challenges to overcome. Production rates are expected to drop from atoms per week for Og down to atoms per year for elements 119 and 120 at modern-day facilities, or atoms per decade for even heavier elements. Lower production cross sections imply longer experiment times, so it is crucial to be able to separate a single atom of a new element from the trillions of other nuclear reaction products that are produced every second. Pairing existing vacuum- or gas-filled separators with updated, highly pixilated detectors provides one avenue toward reducing background from unwanted reaction products.

Another added complication with pushing toward the discovery of new elements is that their lifetimes are expected to decrease rapidly. For instance, predictions for lifetimes of $^{295}119$ and $^{295}120$, the expected $4n$ reaction products from bombarding ^{249}Bk and ^{249}Cf, respectively, with ^{50}Ti beams, are expected to be on the order of just 10 μs [42]. Similar numbers are predicted for $^{298,299}120$, the most likely products of the reaction $^{54}\mathrm{Cr} + ^{248}\mathrm{Cm}$ [43]. These short lifetimes necessitate the move toward digital electronics that can record waveforms and operate almost without dead time, unlike traditional analog electronics.

New element discoveries will benefit greatly from the combined use of highly pixilated detectors coupled to digital electronics. Additionally, looking forward, the SHE field is pursuing several other directions where the same highly pixelated detectors and digital electronics are required, such as high-precision α and γ spectroscopy on SHE nuclides [44–48] and searches for short-lived, neutron-deficient SHE isotopes [49,50].

At the Lawrence Berkeley National Laboratory's (LBNL) 88-Inch Cyclotron facility, the Berkeley Gas-filled Separator (BGS) was designed to investigate the properties of SHEs. Over the last 25 years, the BGS has investigated a wide range of SHE properties, including new isotope production, spectroscopy, mass measurements, and chemistry [51]. In this paper, we present results of the first atom-a-day experiment at the BGS using a new, highly pixelated detector at its focal plane. We explore the $^{244}\mathrm{Pu}(^{48}\mathrm{Ca}, xn)$ reaction, which has previously been investigated at JINR [52,53] and the GSI Helmholtz Center for Heavy Ion Science (GSI) [46–48,54,55]. High-resolution spectroscopy experiments on the α-decay properties of ^{288,289}Fl and their daughters were performed at GSI with TASISpec [46–48]. A comparison of the results from our experiment with those data will provide a useful benchmark for the performance of the BGS detector upgrade. After the description of the experiment in Sec. II, observed correlated decay chains associated with the production of flerovium isotopes are presented in Secs. III A–III D, followed by assessments of magnetic rigidity, decay spectra, random rates and correlations, as well as systematic errors. The paper concludes with a brief summary.

II. EXPERIMENTAL

A $^{48}\mathrm{Ca}^{11+}$ beam was produced from isotopically enriched ^{48}Ca [95.99(2)%] using the Versatile ECR for Nuclear Science (VENUS) ion source [56,57] and injected into the 88-Inch Cyclotron at LBNL. There, it was accelerated to a nominal energy of 256 MeV before being extracted from the cyclotron. The average beam current at the exit of the cyclotron was 8.3 e μA or 4.7×10^{12} ions/s. At the beginning and end of the experimental campaign, the beam energy was

TABLE I. Measured thicknesses of target segments and estimated range of beam energies and excitation through the target according to energy-loss measurements from Ref. [59], experimental masses for ^{48}Ca and ^{244}Pu, along with the theoretical mass for ^{292}Fl from Ref. [60].

Segment	Thickness (mg/cm^2)	Beam energy (MeV)	E^* (MeV)
1	0.39(5)	243.7–238.3	41.2–37.2
2	0.42(4)	243.7–237.9	41.2–36.9
3	0.47(5)	243.7–237.2	41.2–36.3
4	0.45(7)	243.7–237.4	41.2–36.5
Average	0.44(4)	243.7–237.7	41.2–36.7

determined by nondestructively measuring the time-of-flight of individual beam pulses between two fast-current transformers separated by 3.563(5) m along a neighboring beamline [58]. The beam energy was measured to be 258.4(25) and 259.0(25) MeV, respectively. For the experiment, the beam was guided down the Cave 1 beamline and through a differential pumping section that serves to isolate the vacuum of the accelerator beamline from the 0.4-torr He fill-gas inside of the BGS.

Directly following the differential pumping section, the beam impinged on a rotating target wheel composed of four arc-shaped segments with a diameter of 12.2 cm. Each segment consisted of a 2.0(1)−μm-thick ^{nat}Ti foil onto which an average of 0.44(4) mg/cm^2 of ^{244}Pu (as $^{244}PuO_2$) was added via molecular plating. The molecular plating was performed at Lawrence Livermore National Laboratory (LLNL), and the thickness of the ^{244}Pu layer was determined at LLNL through γ-ray analysis of the short-lived ^{240m}Np, which is a daughter in the decay chain of ^{244}Pu. Table I contains a list of measured thicknesses for each target segment and the expected beam and excitation energies for that particular segment. Here, energy losses in the Ti-backing foil and the $^{244}PuO_2$ layer were estimated with srim2013 [59]. The excitation energies were calculated using experimental masses for ^{48}Ca and ^{244}Pu and the theoretical ^{292}Fl mass from the Thomas-Fermi mass tables [60]. The average beam energy in the target was 240.7(30) MeV, leading to an average excitation energy of 39(2) MeV.

Along the length of the differential pumping section, there are five collimators that reduce He pressure along the beamline. These collimators may also reduce the beam intensity on target as compared with that measured at the exit of the cyclotron. Therefore, to extract cross sections, two silicon pin-diode detectors, positioned at angles of $\pm 27.2(1)^\circ$, sit 292(2) mm downstream of the target. These detectors monitor the integral of beam intensity and target thickness through the detection of Rutherford-scattered beam particles. They are used to both monitor the integrity of the target and to provide a normalization to extract the cross section for the nuclear reaction of interest.

During the experimental campaign, the ^{244}Pu target was irradiated for 6.5 days. For the first 24 hours, the beam intensity at the exit of the cyclotron was gradually increased to a maximum of 1 particle μA, with an average intensity of 0.8 particle μA for the remaining time of the experiment. The target was sufficiently thin such that all unreacted beam and reaction products passed through the target and entered the BGS. The Fl evaporation residues (EVR) of interest were separated from the unreacted beam and unwanted reaction products inside the BGS based on their differing magnetic rigidities ($B\rho$) in helium gas [61]. For the first 3.9 days of the experiment, the BGS was set to bend products with $B\rho = 2.25$ T m to the center of the Superheavy Recoil detector (SHREC). This was then increased to $B\rho = 2.34$ T m for the remainder of the experiment. The $B\rho$ settings of the BGS were previously calibrated with beams of various known magnetic rigidities, observing what combinations of magnetic settings were required for the two dipole magnets to center each beam at the focal plane. This calibration allows us to calculate the $B\rho$ for a wide range of dipole ratios (see Sec. III E).

At the BGS focal plane, the separated EVRs were implanted into the newly constructed SHREC detector, which has been described in detail in Ref. [62]. SHREC consists of an implantation detector that is comprised of three double-sided silicon-strip detectors (DSSDs), each with an active area of 58.5 mm × 58.5 mm, a thickness of 325 μm, and an average deadlayer thickness of ≈1.5 μm. Each DSSD is subdivided into 58 strips on both the front and back sides. These three DSSDs are situated side-by-side and perpendicular to the path of the beam. On the front side of the detector, the 174 vertical strips denote position in the horizontal direction. On the back sides of the implantation detector, the 58 strips were wire-bonded across all three DSSDs, yielding 58 strips that denote the vertical position.

Some light, high-energy, charged particles generated from reactions between the beam and the He fill-gas pass through the implantation detector, depositing only a portion of their energy in the implantation detector and can mimic α particles. To better discriminate between these "punch-through" particles and the α decays, a veto detector was positioned directly downstream of the implantation detector and is comprised of an identical set of three DSSDs (see Sec. III F).

Some fraction of α particles will be emitted out of the face of the implantation detector. To detect a portion of these emitted particles, an additional eight DSSDs comprised a "tunnel" of detectors directly upstream of the implantation detector. The geometric efficiency for detecting a full-energy α particle in the implantation detector is ≈50%. An additional 25%–30% of α decays can be reconstructed between the implantation detector and upstream detectors, depending on the implantation profile. Combined, this leads to an overall α-particle detection efficiency of 75%–80% [62].

Note that this experiment did not employ any parallel-plate avalanche counter (PPAC) or multiwire proportional counter (MWPC) upstream of SHREC to tag potential EVR events as originating from the separator as opposed to random background. This choice is different from many other experimental setups that investigate SHE. However, this decision was made because early experiments have demonstrated that EVR collection efficiency was reduced by 10%–15% when a PPAC is installed. In turn, the beam-related background in the BGS is low, such that decay chains from $^{287-289}$Fl, the expected decay products of this experiment can be definitively identified

without the need for the PPAC. This is discussed further in Secs. III G and III H. Under these experimental conditions, the efficiency for transport of the Fl EVRs to SHREC is 62(6)%, based on simulations of particle trajectories in the BGS and assuming that the Fl EVRs were centered in SHREC [61].

Individual signals from each DSSD strip were processed with compact, charge-sensitive preamplifiers [63] and then sent to ten 64-channel CAEN VX2740 digitizers (16 bit, up to 125 MS/s). Each digitizer channel self-triggered above an energy threshold of $\gtrsim$200 keV. Signals were processed using the Digital Pulse Processing Pulse Height Analysis (DPP-PHA) firmware controlled through the compass software from CAEN [64]. Waveforms [40 μs long on the back sides (horizontal strips), 30 μs long on the front sides (vertical strips)], timestamps, detector strip identifiers, and pulse amplitudes from an online trapezoidal filter were recorded for all events [62]. Energy calibrations were performed for SHREC before the experiment using α sources consisting of ^{239}Pu, ^{241}Am, and ^{244}Cm, and a ^{207}Bi conversion-electron source. The utilized calibration technique was previously optimized using α-decay lines of implanted ^{254}No, ^{250}Fm, and ^{246}Cf. To correct for potential-energy shifts during the experiment, an α source consisting of ^{239}Pu, ^{241}Am, and ^{244}Cm was located inside the chamber and in sight of most strips for the duration of the experiment. This source was located in a position such that it did not occlude the EVR envelope or decrease detection efficiency. At the relevant decay energies, the in-beam resolution of the DSSD during the experiment was 10 keV at (one sigma) for alpha particles that decayed into the DSSD and approximately 20 keV (one sigma) for alpha particles that were reconstructed between the DSSD and the box detector, although this depends on the angle between the two detectors and how much dead layer the alpha particle passes through. The resolution was determined by measuring the resolution of ^{254}No alpha decays in a commissioning experiment performed several months prior to this experiment. In fact, the calibration could be monitored using the decay of the long-lived ^{242}Cm daughter of ^{254}No to ensure there were no energy drifts between the two experiments. No energy drift was observed in any detector strip that contained an event attributed to a Fl decay chain.

III. RESULTS AND DISCUSSION

The expected reaction products of this experiment were the $3n$ and $4n$ exit channels, ^{289}Fl and ^{288}Fl, respectively. Both of these isotopes have been studied previously, either through direct production or as the daughters of ^{292,293}Lv, in experiments at the Dubna Gas Filled Recoil Separator (DGFRS) at JINR [52,65–67], the Transactinide Separator and Chemistry Apparatus (TASCA) at GSI [46–48,54,55,68,69], the velocity filter SHIP at GSI [70], and the GARIS gas-filled separator at RIKEN [71]. The accumulated known decay properties [46,47] from these experiments are summarized in Fig. 1. For completeness, Fig. 1 also contains accumulated known decay properties of ^{286,287}Fl: Decay chains passing through ^{286}Fl, including recent data from JINR [72], have recently been assessed in the Supplemental Material of Ref. [40]. Decay chains passing through ^{287}Fl, including recent data from JINR [72], are assessed in the Supplemental Material of this article [73] (including references [74,75]).

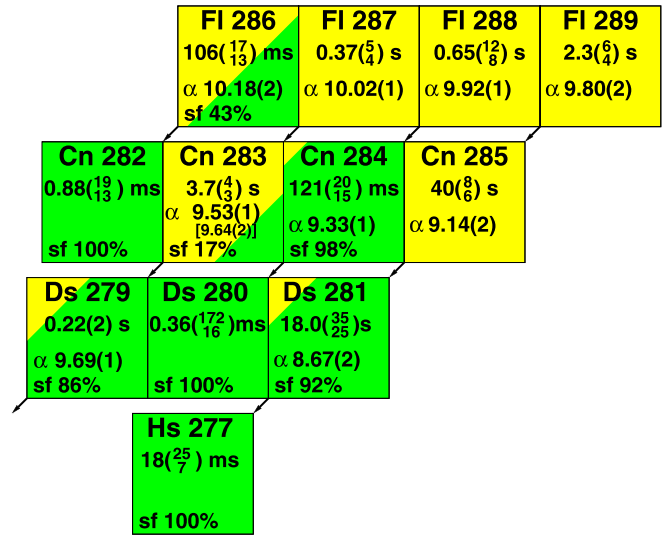

FIG. 1. Known decay properties of ^{286,287,288,289}Fl and their descendants. The values for the decay chain starting from ^{286}Fl are taken from the Supplemental Material of Ref. [40]. The values for the decay chain starting from ^{287}Fl are taken from the Supplemental Material of this article [73]. The values for the decay chain starting from ^{288}Fl are taken from the Supplemental Material of Ref. [46]. The values for the decay chain starting from ^{289}Fl are taken from the rightmost column of Table II in the Supplemental Material of Ref. [47]. For updates, including data from this article, see Table III and the Supplemental Material [73].

A. Search conditions

Prior to this experiment, SHREC was commissioned using the ^{208}Pb(^{48}Ca, $2n$) reaction. The ^{254}No EVRs from that reaction had a median energy of 19.2 MeV with recorded energies ranging from approximately 14 to 25 MeV. Based on differing reaction kinematics and simulations from srim [59], we expected the Fl EVRs to implant into SHREC with comparable or slightly lower recorded energies. Using this information, and the known reference decay chains originating from Fl isotopes shown in Fig. 1, potential decay chains originating from ^{288}Fl were identified from a larger subset of correlations which met the required conditions of the implantation of an EVR [$11 \leqslant E(\text{MeV}) \leqslant 30$] followed by either an α-like [$8 \leqslant E(\text{MeV}) \leqslant 11$] or escape-like [$E(\text{MeV}) \leqslant 5$] event and terminated with a spontaneous fission (SF) event ($E \geqslant 120$ MeV) within 10 s. All three events must occur within the same (x, y) pixel of the implantation detector. The EVR was required to be anticoincident with the veto detector. The α, escape, or SF events could be coincident with the veto detector because conversion electrons emitted during the decay may pass through the implantation detector and into the veto detector, creating a real coincidence. A coincidence between the implantation detector and veto detector is defined as a signal that occurs in the veto detector within 1 μs of a signal in the implantation detector and within ±2 mm of the implantation position in both the x and y directions. The

TABLE II. Observed decay chains associated with isotopes of flerovium, $Z = 114$. Reconstructed α-decay energies are noted with italics. SF energies, shown in boldface, correspond to energies measured in the implantation and upstream tunnel detectors, respectively.

E^* (MeV)	E_{beam} (MeV)	Chain Number	x strip	y strip	$B\rho$ (T m)	E_{EVR} (MeV)	Decay energy (MeV)	Correlation Time (s)	Isotope ^AZ
41.2–36.7	243.7–237.7	1	135	17	2.25	12.6	9.91(1)	0.121	^{288}Fl
							166 + 2	0.0256	^{284}Cn
41.2–36.7	243.7–237.7	2	141	3	2.25	14.3	*9.92(2)*	0.289	^{288}Fl
							189 + 19	0.0334	^{284}Cn
41.2–36.7	243.7–237.7	3	92	34/35	2.34	15.0	*9.94(2)*	0.645	^{288}Fl
							177 + 7	0.783	^{284}Cn
41.2–36.7	243.7–237.7	4	104	31	2.34	18.1	0.71	0.628	^{288}Fl
							146 + 2	0.00470	^{284}Cn
41.2–36.7	243.7–237.7	5	77	27	2.34	14.5	*9.92(2)*	0.115	^{288}Fl
							192	0.0390	^{284}Cn
41.2–36.7	243.7–237.7	6	84	9/10	2.34	16.6	*9.92(2)*	0.0268	^{288}Fl
							169 + 14	0.0841	^{284}Cn
41.2–36.7	243.7–237.7	7	118	18	2.34	17.1	9.92(1)	2.55	^{288}Fl
							197	0.0939	^{284}Cn
41.2–36.7	243.7–237.7	8	87	21	2.25	19.1	9.98(1)	0.665	^{287}Fl
							9.65(2)	9.07	^{283}Cn
							154	0.0157	^{279}Ds
41.2–36.7	243.7–237.7	9	98	6	2.25	19.8	1.20	1.16	^{289}Fl
							9.16(1)	158	^{285}Cn
							216	35.7	^{281}Ds
41.2–36.7	243.7–237.7	10	84	3	2.34	Missing			Missing
							9.22(1)	10.6-37.5	^{285}Cn
							7.99(1)	489	^{281}Ds
							211 + 2	0.120	^{277}Hs

efficiency for detecting a decay chain originating from ^{288}Fl under these conditions is ≈99 %, based on Monte Carlo simulations of decay chains with branching ratios, as shown in Fig. 1.

Potential decay chains originating from ^{289}Fl were also identified by EVR-α-SF correlations. The same energy conditions as for ^{288}Fl were applied, while the time difference between the EVR- and SF-like events was extended to $\leqslant$300 s, and at least one full-energy α particle [$8 \leqslant E(\text{MeV}) \leqslant 11$] was required to be observed between the EVR and SF-like events. The efficiency for detecting a decay chain originating from ^{289}Fl under these conditions is ≈99%, based on Monte Carlo simulations of decay chains with branching ratios, as shown in Fig. 1.

We also searched for potential events originating from the decay of ^{287}Fl, the 5n exit channel. Decay chains originating from ^{287}Fl were identified by correlations consisting of either an EVR followed by an α-like event and terminated by an SF-like event within 10 s, or an EVR-like event followed by at least two α-like events within 150 s and terminated by an SF-like event within an additional 2.5 h.

B. ^{288}Fl Decay chains

Seven EVR-α-SF correlations were observed and assigned to the decay of ^{288}Fl. Their decay properties are summarized in Table II. A comparison between the decay properties observed in this work and those from previous publications is shown in Fig. 2. The half-life originating from the decays in this work is $0.43(^{26}_{12})$ s for the decay of ^{288}Fl and $36(^{22}_{10})$ ms for ^{284}Cn. The observed half-life of ^{288}Fl is in very good agreement with data from previous publications, while the observed half-life of ^{284}Cn is approximately three sigma away from the value $T_{1/2} = 121(^{20}_{15})$ ms, shown in Fig. 1, which corresponds to an aggregation of all known decays assigned to ^{284}Cn, as detailed in the Supplemental Material of Ref. [46]. As can be seen in the figure, the correlation times observed in this work are within the range of times that have been previously observed, although trending toward lower values. This deviation is likely due to statistical fluctuations that are common for experiments with a small number of events.

Our data indicate that ^{288}Fl predominately decays via the emission of a 9.92(1)-MeV α particle, in perfect agreement with what was reported in Ref. [46]. This can be seen in the overlap of α-particle energies from this work and Ref. [46] that is highlighted in Fig. 2(a) in the "TASISpec only" curve. It is noticeable that the distribution of energies observed in this work and Ref. [46] is significantly narrower than those observed in previous works. Consequently, and in line with Ref. [46], the narrow α energy observed in this work does not support the suggestion from Ref. [76] that proposed two close-lying decay paths, each with similar strength, differing by only ≈100 keV after analysis of data from Refs. [54,55,70]. This highlights the need for experiments on SHEs that leverage high-resolution spectroscopic techniques, which may be able to resolve similar deviations in other SHE isotopes and lead

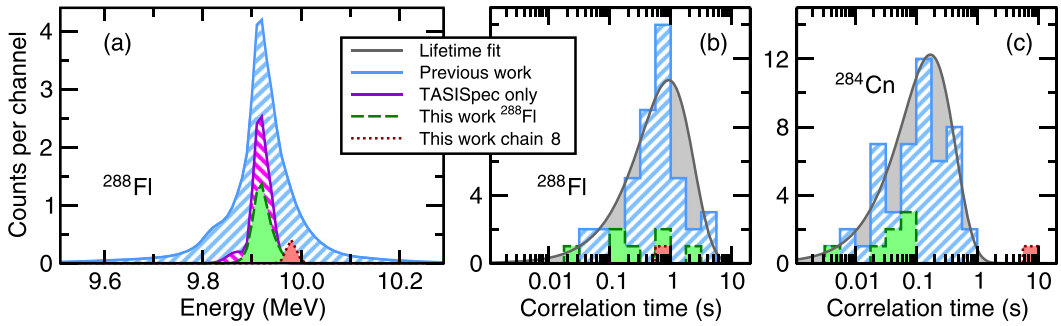

FIG. 2. Comparison of (a) decay energies and (b) correlation times associated with the decay of ^{288}Fl, as well as (c) correlation times associated with the subsequent decay of ^{284}Cn. The energy spectra in panel (a) are based on sums of Gaussian distributions accounting for varying uncertainties of the different experiments. For all panels, the blue hash curves correspond to all previous work as summarized in Ref. [46]. Data from decay chains associated in the present work with ^{288}Fl are indicated in green and those from chain 8 in red (cf. Table II). In panel (a), the spectroscopic results from the TASISpec detector at TASCA [46] are denoted by the hashed maroon curve. In panels (b) and (c), the gray curves correspond to least squares lifetime fits to all previous data [46].

to a better understanding of the underlying nuclear structure in these exotic systems [77].

It has previously been reported that there is a small α branch in ^{284}Cn of about 2 % with an energy of $E_\alpha =$ 9.33(1) MeV [46]. This α-decay branch was not observed in this work as all nuclei of ^{284}Cn were observed to undergo SF.

The information from the present work was used to update the aggregated data of ^{288}Fl decay chains. This is summarized in Table III and detailed in the Supplemental Material [73]. Each decay step is found to remain consistent with the decay of a single radioactivity according to Ref. [79].

The cross section for the observation of seven events of the 4*n* exit channel is 6.7$(^{36}_{25})$ pb. This value compares favorably to the reported cross sections of 9.8$(^{39}_{31})$ pb [55], 5.3$(^{36}_{21})$ pb [80], and 5.1$(^{29}_{21})$ pb [48], which are published values for the same reaction and at similar compound nucleus excitation energies.

C. Decay chains 9 and 10: ^{289}Fl

Chain 9 in Table II consisted of a 19.8-MeV EVR followed 1.155 s later by an escape-like event. There was a 9.16-MeV α-like event 157.6 s after the escape-like event, and the chain was terminated by an SF-like event that occurred 35.7 s after the last α-like event. A comparison of these decay properties to aggregated numbers from all the decay chains assigned to ^{289}Fl suggests that the observed decay characteristics of chain 9 are all consistent with the so-called main decay branch of ^{289}Fl [47]. This is illustrated in Fig. 3, where the data points belonging to chain 9 are indicated in green and the dashed line. Additionally, the energy of the escape-like event is consistent with the energies expected for the energy imparted in the DSSD for an α particle escaping the implantation detector,

TABLE III. Summary of aggregated experimental results concerning the decays of ^{288}Fl and ^{284}Cn accounting for the additional data from this work. See Supplemental Material for more details [73].

Isotope ^{A}Z	E_α (MeV)	Q_α (MeV)	$T_{1/2}$ (s)	b_α	$T_{1/2}(\alpha)$[a] (s)	HF[a] [78]	$T_{1/2}$(SF)[a] (ms)
^{288}Fl	9.92(1)	10.06(1)	0.62$(^{10}_{8})$	1	0.62$(^{10}_{8})$	1.5$(^{4}_{3})$	n/a
^{284}Cn	9.33(1)	9.46(1)	0.110$(^{17}_{13})$	1/58	6.4$(^{10}_{8})$	1.1$(^{3}_{2})$	0.112$(^{17}_{13})$

[a]The uncertainties do not account for uncertainties in branching ratio.

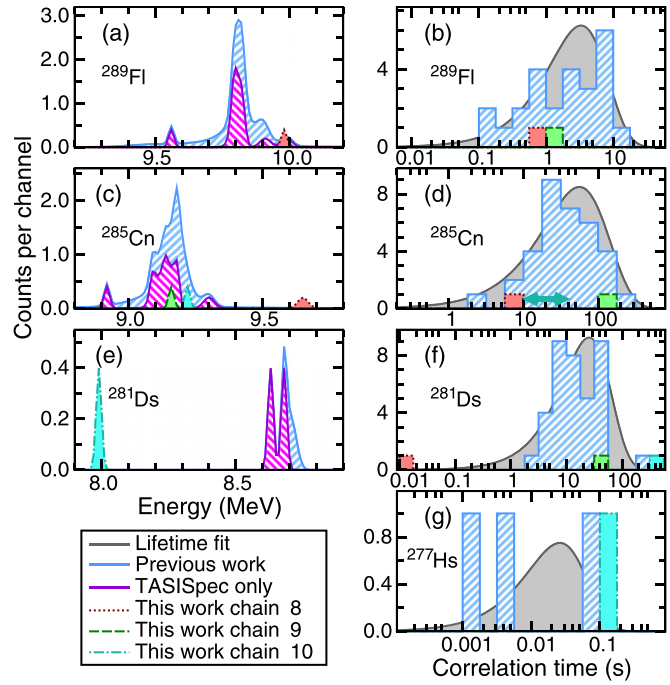

FIG. 3. Comparison of α-decay energies and correlation times of ^{289}Fl [panels (a) and (b)], ^{285}Cn [panels (c) and (d)], ^{281}Ds [panels (e) and (f)], and correlation times of ^{277}Hs [panel (g)]. Decay energies and correlation times from all previous work at the DGFRS [52,53,65,66], TASCA [47,48,54,55,68,69], SHIP [70], and GARIS [71] separators are denoted with blue hashed histograms. They correspond to assessments detailed in the Supplemental Material of Ref. [47]. The energy spectra in panels (a), (c), and (e) are based on sums of Gaussian distributions accounting for varying uncertainties of the different experiments. Here, the spectroscopic results from the TASISpec detector at TASCA [47,48] are denoted by the hashed maroon curve. In panels (b), (d), (f), and (g), the gray curves correspond to least squares lifetime fits to all previous data [47]. Data from decay chains 8, 9, and 10 from the present work (cf. Table II) are shown in red, green, and turquoise, respectively.

TABLE IV. Timeline of actions before and during chain 10.

Action	Time
Data acquisition stopped	11:31:02:002 (UTC)
File change in progress	No data recorded
Data acquisition started	+26.967 s
9.22(1) MeV α-like event	+10.563 s
7.99(1) MeV α-like event	+489.068 s
213 MeV SF-like event	+0.120 s

as can be seen in Fig. 2 of the Supplemental Material of Ref. [48]. The lifetimes of all three decays are well within the range of previously recorded values for ^{289}Fl, ^{285}Cn, and ^{281}Ds. Additionally, the energy observed for the α decay in this work is in good agreement with the energies from decays previously assigned to ^{285}Cn [47]. As such, this decay chain 9 was assigned to the decay of ^{289}Fl.

Chain 10 in Table II was initially discovered when searching backward from all 78 observed SF-like decays. During that search, an $\alpha-\alpha$-SF correlation consisting of two α particles of 9.22(1) and 7.99(1) MeV, respectively, was identified. The time difference between the two α particles amounts to 489 s. The second α particle was followed by a 213-MeV SF-like event only 120 ms later. The SF-like event was coincident with a signal in the veto detector, which may occur when a conversion electron is emitted toward the veto detector during SF-decay. This was the only event with $E \geqslant 120$ MeV coincident with a signal in the veto detector. A dedicated search backward in time from the first α-like event does not show any evidence of an EVR or additional, previous α-decay events. Further investigation showed that the first α-like event occurred only 10.563 s after a new runfile had been started. A timeline of the events that are discussed in the following sentences can be seen in Table IV.

Runfiles are manually stopped and started roughly every 2 h, and there is a small, but inescapable, time during this process when the data acquisition system is not running. Analysis of the online file information shows that one file was closed April 26, 2023 at 11:31:02.002 UTC. The next file, containing the $\alpha-\alpha$-SF correlation of interest, was not opened and collecting data until 26.967 s later. During this time, the beam was not stopped and was still impacting the target. A random rate analysis was performed as discussed in Sec. III G. Those calculations indicated that the probability of two alpha-like events occurring within 2000 s of an SF-like event is 7.1×10^{-5}. Therefore, the correlation is unlikely to be random.

This chain is tentatively interpreted as originating from ^{289}Fl, where the EVR implantation and ^{289}Fl decay happened while runfiles were being changed. The subsequent α decays of ^{285}Cn and ^{281}Ds, along with the SF of ^{277}Hs occurred after the new file was open. The correlation time of the potential ^{285}Cn decay has to be in the range $\Delta t = 10.6-37.4$ s. This period, indicated by a horizontal turquoise double-arrow in Fig. 3(d) and the observed α-particle energy of $E_\alpha =$ 9.22(1) MeV are both consistent with the known decay properties of ^{285}Cn summarized in Ref. [47].

^{281}Ds has previously only been observed to decay via α-particle emission three times. The α-particle energy assigned to the decay of ^{281}Ds in this work is lower than what has been previously observed. However, it could indicate observation of a decay into an excited state in the ^{277}Hs daughter, or decay from a lower-lying state in ^{281}Ds. A third alternative is an α-decay measurement with part of the energy lost in the deadlayer of the implantation detector. The correlation time of the α decay assigned to ^{281}Ds in this work is 489 s. This is significantly longer than the average half-life shown in Fig. 1(f) of $T_{1/2} = 18.0(^{35}_{23})$ s [47]. However, it is notable that the observed correlation time of one of the three observed α-decay events assigned to ^{281}Ds is 252 s [47], which is consistent with the lifetime observed here. This could indicate the existence of a longer-lived isomeric state in ^{281}Ds. The correlation time of the observed SF event that followed the α-decay assigned to ^{281}Ds is consistent with the lifetimes from the other known decays assigned ^{277}Hs [see Fig. 3(g) and Ref. [47]]. Including the two ^{289}Fl chains of this work, the revised aggregated half-lives of ^{281}Ds and ^{277}Hs shift toward larger values of $26(^{5}_{4})$ s and $35(^{35}_{12})$ ms, respectively, while the spread of data points remains consistent with only one radioactive decay for each of these two decay steps (see Supplemental Material [73]).

The cross section observed for two decays of the $3n$ exit channel, ^{289}Fl, was $1.6(^{22}_{11})$ pb. Previous experiments at the DGFRS [53] and TASCA [54,55] reported cross sections of $1.7(^{25}_{11})$ and $3.5(^{33}_{20})$ pb, respectively. Our value agrees well with these values, while the TASISpec experiment at TASCA indicates a somewhat higher cross section of $6.2(^{32}_{24})$ pb for the $3n$ channel ^{289}Fl [48]. All measurements were undertaken at comparable compound nucleus excitation energies.

We have considered the possibility that the difference in cross section between this work and that of TASISpec may be due to a larger difference in beam energies than reported. For this experiment, we measured the beam energy on a neighboring beamline, then switched the beam to the beamline leading to the BGS. During this process, minor modifications need to be made to the tune of the cyclotron. These modifications may have minor impacts on the energy of the extracted beam by taking out an earlier or later turn through the cyclotron. For this experiment, each turn out of the cyclotron added an additional $\approx$1.5 MeV. After this experiment was completed, two fast-current transformers [58] were installed on the beamline that leads to the BGS to allow online time-of-flight (TOF) measurements between individual beam pulses. This setup was commissioned using beams of ^{40}Ar^{10+} and ^{50}Ti^{12+}. Energy measurements were compared between the two beamlines, and the energy on the beamline leading to the BGS was consistently $\approx$1 MeV lower than the energy measured on the neighboring beamline, although this may be due to a more accurate measurement of the TOF distance on the Cave 1 beamline. Based on the small energy difference, we conclude that the $2-\sigma$ differences in cross-section measurements are statistical fluctuations.

D. Decay chain 8: ^{287}Fl

Chain 8 in Table II consisted of an EVR-$\alpha-\alpha$-SF correlation where the EVR was followed 0.665 s later by a 9.98-MeV α particle. A second α with 9.65 MeV followed 9.073 s later, and the chain was terminated by an SF just 16 ms after the second α. The excitation energy covered by the target during this experiment was calculated to be 36.7–41.2 MeV (see Table I). Based on this, we expected to observe decay products originating from the $3n$ (^{289}Fl) and $4n$ (^{288}Fl) exit channels. A comparison of the decay properties observed in this chain with those from all previous decay chains assigned to ^{288}Fl and ^{289}Fl are shown in Figs. 2 and 3, respectively.

When comparing the decay properties observed in chain 8 with the known properties of ^{289}Fl, note that the first and second α-decay correlation times are consistent with the known decays from ^{289}Fl and ^{285}Cn [47]. Additionally, the energy of the first α particle could also be consistent with ^{289}Fl, although only one other decay has been observed at an energy of $E_\alpha \approx 9.99$ MeV. However, the energy of the second α particle is $\gtrsim$300 keV higher than any previously observed α decay of ^{285}Cn. Furthermore, the correlation time of the SF-like event is two orders of magnitude shorter than any decays assigned to ^{281}Ds. Therefore, it is unlikely that chain 8 originates from the decay of ^{289}Fl.

The same comparison was performed between this chain and the known decays originating from ^{288}Fl shown in Fig. 2. While the first α particle has an energy and lifetime that is consistent with the published decay properties of ^{288}Fl, the lifetime of the Cn α decay in chain 8 is significantly longer than any previously published value [46]. Additionally, our observed energy of $E_\alpha = 9.65(2)$ MeV does not agree with the previously observed α-particle energy for ^{284}Cn of $E_\alpha = 9.33(1)$ MeV. The SF correlation time of 16 ms is also significantly longer than can reasonably be expected to occur from the decay of ^{280}Ds, which has been observed to under SF in $\approx$0.36 ms. Therefore, we cannot assign chain 8 to the decay of ^{288}Fl.

We also compared the decay properties for chain 8 to the decay properties of chains assigned to ^{287}Fl and its descendants. This is shown in Fig. 4 and detailed in the Supplemental Material [73]. There is good agreement between α-particle energies and correlation times for all three generations of decays. As such, we assigned chain 8 to the decay of ^{287}Fl. An interesting side note on nuclear structure is that the observed 9.65(2) MeV of the ^{283}Cn α agrees well with several previously measured decay events following indirect population of ^{283}Cn, while the decay-energy spectrum of directly produced ^{283}Cn does not show any clear evidence of such an α-decay transition (see Fig. 2 of the Supplemental Material [73]).

In the ^{48}Ca + ^{244}Pu reaction, the isotope ^{287}Fl would be produced in the $5n$ exit channel. While the $5n$ exit channel has been observed in reactions between ^{48}Ca and actinide targets before [53,83,84], no decays from a $5n$ exit channel have been observed at compound nucleus excitation energies less than 50 MeV. This is a significantly higher excitation energy than what was the case for our target (36.7–41.2 MeV, see Table I) and cannot be explained by small deviations between experimental methods of determining excitation energies for a given experiment. We also considered whether our beam energy measurement could be off due to measuring the beam energy on a neighboring beamline. As discussed in Sec. III C, we expect a systematic offset of at most $\approx$1 MeV for the beam energy, which would still yield an excitation energy that is significantly lower than what has previously been observed for $5n$ exit channels. Another way that ^{287}Fl could be produced is through the ^{242}Pu(^{48}Ca, $3n$) reaction if ^{242}Pu is present in the target as a contaminate. The target material was assayed and determined to be 98.8 % ^{244}Pu and 0.91 % ^{242}Pu by atom%. All other Pu isotopes contributed $\lesssim$1% of the target material by atom%.

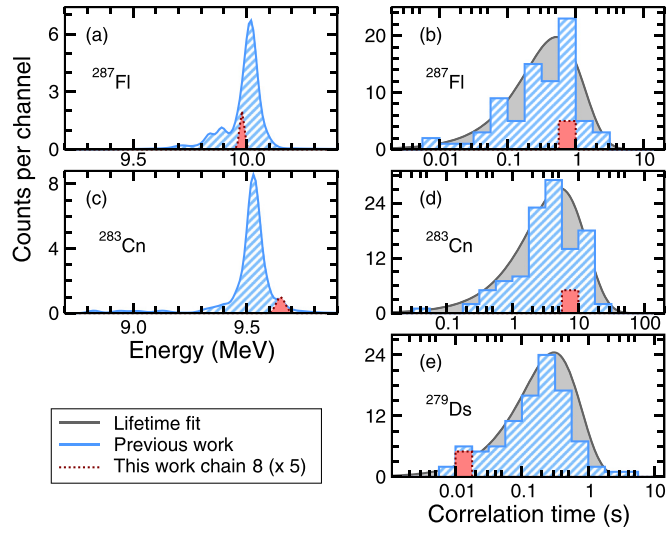

FIG. 4. Comparison of (a) α-particle energies and (b) correlation times of ^{287}Fl, (c) α-particle energies and (d) correlation times of ^{283}Cn, and (e) ^{279}Ds SF and α-particle correlation times between chain 8 in this work and from previous work. Previously measured α-particle energies at the DGFRS [53,72,80], SHIP [81], and BGS [82] separators are denoted with blue hashed histograms, and correlation times from those works are denoted by light-gray histograms. Data from Chain 8 (multiplied by 5 in yield for better visibility) from this work is denoted by the red histograms. See the Supplemental Material [73] for further details on aggregated results.

E. Magnetic rigidity ($B\rho$)

Two $B\rho$ settings were used to tune Fl ions to the SHREC detector. The location of where the events were observed at both of the $B\rho$ settings is shown in Fig. 5(e). The first setting was $B\rho = 2.25$ T m and two of the events from ^{288}Fl as well as chains 8 and chain 9 assigned to ^{287}Fl and ^{289}Fl, respectively, were observed with these settings. All four events were implanted on the high-$B\rho$ side of SHREC. Based on the known dispersion of the BGS of 16(2) mm/%($B\rho$), the average of these four events was $B\rho = 2.33(3)$ T m. After observation of these events, the $B\rho$ setting was increased to 2.34 T m, where the remaining six events were observed. The average magnetic rigidity of all ten events was 2.35(2) T m. Previous experiments at TASCA have observed $B\rho = 2.29(15)$ T m for flerovium residues [55], and experiments with TASISpec and chemistry at TASCA have used

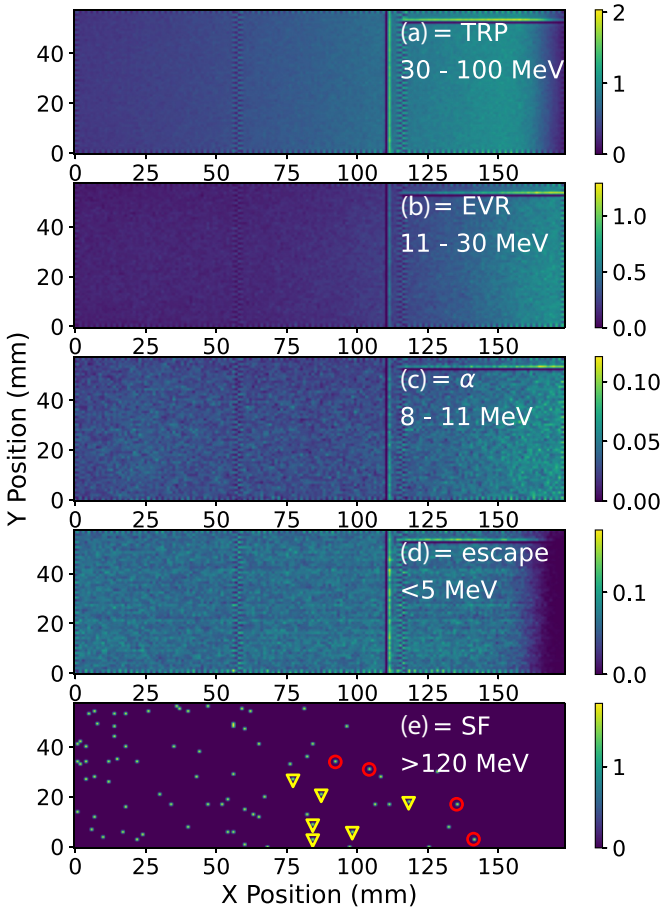

FIG. 5. Distribution of (a) TRP-like, (b) EVR-like, (c) α-like, (d) escape-like, and (e) SF-like events in the implantation detector of SHREC. The heatmap shows the rate per pixel per 1000 seconds for each background component in panels (a)–(d) and the observed location of every SF event in panel (e). The location of observed correlations associated with flerovium decay chains at $B\rho = 2.28$ and $B\rho = 2.34$ are also indicated in panel (e) with red circles and yellow triangles, respectively.

$B\rho = 2.27$ T m. A small discrepancy between the $B\rho$ at the two separators may be due to the different gas pressures that are used at each separator. TASCA is operated at 0.6 torr compared with the BGS setting of 0.5 torr, although $B\rho$ is expected to be relatively constant over this range [61]. Another potential cause of the discrepancy may be due to different methods of calibrating $B\rho$. The BGS has two dipole magnets, M1 and M2, that bend the EVRs ≈25° and ≈45°, respectively, but this can be varied to better tune for specific experiments. To calibrate the BGS magnets, beams of $^{40}Ar^{13+}$ at several different energies were sent through the BGS, to the focal plane detector, when the BGS was at vacuum. The settings of the M1 magnet were set, and the M2 value was varied until the beam was centered at the focal plane of the BGS. This was done for 10–20 different settings of M1 at each beam energy. The resulting data allow us to determine experimental $B\rho$ from a wide range of magnet settings. This may be different than the method employed at TASCA and may explain the small variation in observed $B\rho$ values.

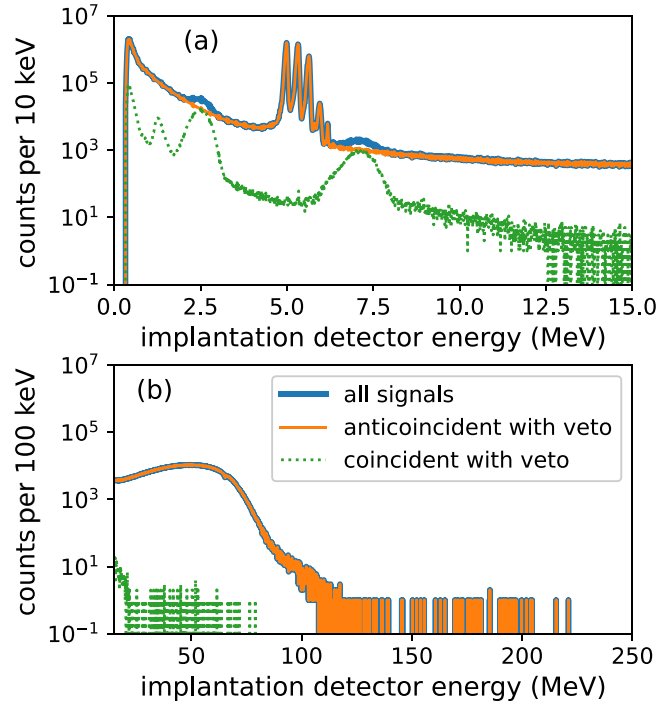

FIG. 6. All events in the SHREC detector from (a) $0 \leqslant E(\text{MeV}) \leqslant 15$ and (b) $E \geqslant 15$ MeV. Each panel shows the total summed events (thick solid, blue), events that are coincident with the veto detector (dotted, green), and events that are anticoincident with the veto detector (thin solid, orange).

F. Spectra

The low- $[0 \leqslant E(\text{MeV}) \leqslant 15]$ and high-energy ($E \geqslant 15$ MeV) spectra, summed across all strips in the implantation detector, from this experiment are shown in Figs. 6(a) and 6(b), respectively. The high-energy spectrum shows a broad peak at ≈50 MeV that is caused by target-like material and target-like transfer reaction products (TRP) that are ejected from the target during irradiation and implanted into the detector. Above 100 MeV, the spectrum is dominated by a small amount of scattered beam particles that hit the implantation detector, along with SF events from the Fl decay chains. Also shown in Fig. 6(b) is the spectrum of all signals that are coincident with the veto detector, meaning that a signal that occurred in the veto detector within 1 μs of a signal in the implantation detector and within ±2 mm of the implantation position in both the x and y directions. Only one event above 100 MeV in the implantation detector was coincident with a signal in the veto detector and was discussed in Sec. III C.

The low-energy spectrum shows background from several sources. For the duration of the experiment, a multipeak α source was located in the SHREC chamber, pointing toward the implantation detector. This source was used to track any potential-energy drifts in the electronics during the beamtime. The peaks from this source can be seen at $5 \lesssim E(\text{MeV}) \lesssim 6$. Each peak is broad in energy as the source was on the edge of the detector, and the deadlayer traversed by the α particles varied depending on the angle and the distance between each pixel and the source. A narrow peak occurs at 6.16 MeV and

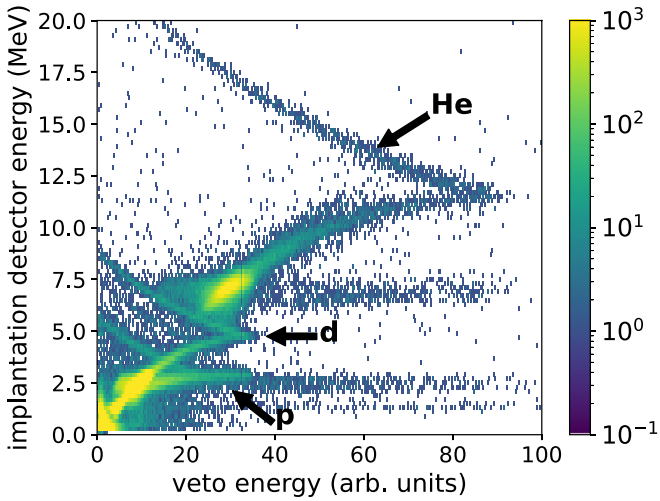

FIG. 7. Energy loss through the implantation detector and veto detector for ions that pass through the implantation detector. They deposit only a fraction of their energy in the implantation detector, which thus acts as the ΔE part of a $\Delta E - E$ particle-identification telescope. The location of particles originating from elastically scattered He fill gas (solid line), deuterons (dotted line), and protons (dashed line) is indicated.

is from the decay of ^{242}Cm ($T_{1/2} = 162.86$ d). This isotope is part of the decay path of ^{254}No, which was implanted into SHREC in October 2022 during commissioning of the detector via the ^{208}Pb(^{48}Ca, $2n$) reaction.

Three additional, very broad peaks show up in the low-energy spectrum centered at ≈1, 3, and 7 MeV. These are the appropriate energies to mimic either escape-like or full-energy α-like signals. The vast majority of the events associated with these peaks are coincident with signals in the veto detector and are expected to originate from high-energy light charged particles that pass through the implantation detector. As shown in Fig. 6(a), background from these events can be removed by selecting only those events in the implantation detector that are anticoincident with the veto detector. Recall that all of our EVR events were required to be anticoincident with the veto detector.

To better understand the sources of the three broad peaks that are coincident with the veto detector and at ≈1, 3, and 7 MeV, the correlated energy-loss measurements of both the implantation and veto detector are shown in Fig. 7. Based on comparisons with simulations from srim [59], the particles originate primarily from protons, deuterons, and α particles as indicated in Fig. 7. The helium background is mainly a result of elastically scattered BGS fill-gas particles, while the protons and deuterons likely are emitted from the target area or the beamstop due to the impinging of or reactions with the high-intensity primary beam, respectively.

G. Random rates

The number of expected decay chains arising from correlations of random background events was calculated for each pixel individually, based on the rate of events within a given energy range in that pixel, for each ≈2-hr data file. Then the rates observed for each pixel were summed across the entire detector to give the total random rate for each event type.

EVR-like events were defined as those with $11 \leqslant E_{\mathrm{EVR}}(\mathrm{MeV}) \leqslant 30$, with α-like events having $8 \leqslant E_{\alpha}(\mathrm{MeV}) \leqslant 11$ and SF events having energies of $E_{\mathrm{SF}} \geqslant 120$ MeV. The energy threshold for SF events for this experiment was determined based on the observed energies neutron-deficient Db SF decays produced in the ^{209}Bi(^{50}Ti, xn) reaction and implanted into this detector. The distributions of EVR-, α-, and SF-like events across the detector are shown in Figs. 5(b), 5(c), and 5(e), respectively. The median rate of EVR-like events was 7.2×10^{-5} Hz/pixel, with lower rates observed for lower x positions. In SHREC, lower x positions correspond to particles that have a lower $B\rho$ and are bent more by the BGS magnets. Background from α-like events was found to be more evenly distributed across SHREC. The median rate was 3.2×10^{-5} Hz/pixel. A total of only 78 SF-like events were observed in SHREC during the whole experiment. Their distribution is shown in Fig. 5(e). The SF-like events were primarily observed at lower x positions and are likely the result of a tiny amount of beam scattering off the beamstop that runs along the low $B\rho$ side of the BGS vacuum chamber, and then impacting the detector. No short-lived SF activity potentially due to actinide isomers impacting SHREC was observed, which will be discussed in Sec. III H.

The other two sources of background in SHREC are target-like recoil products (TRP) with $30 \leqslant E(\mathrm{MeV}) \leqslant 100$ and escape-like events defined as $E_{\mathrm{esc}} \leqslant 5$ MeV. The upper limit for escape-like events was limited by background from an α source (^{239}Pu, ^{241}Am, ^{244}Cm) that was in the detector box and emitted 5 to 6 MeV α particles. The threshold for escape-like events was set below the energies of these α particles to reduce potential random coincidences from these known background events. The observed distributions of these events across SHREC are shown in Figs. 5(a) and 5(d), respectively. Escape-like events are relatively evenly distributed across the implantation detector and occur with a median rate of 0.024 Hz/pixel. Recoiling TRP have lower $B\rho$ than EVRs and bend more in the BGS magnets, however, background from these events was observed primarily to occur at the high-$B\rho$ side of the detector. This may be due to TRP scattering off the beamstop. Some other contributions of events in this energy range may also be from beam particles that have deeper interactions within the beamstop and scatter into the SHREC implantation detectors. The TRP-like events have a median rate of 5.7×10^{-4} Hz/pixel, slightly higher than the rate observed with EVR-like events.

The number of expected correlations between random events that could be incorrectly identified as decays originating from $^{288-289}$Fl was calculated per pixel, for each 2-h runfile, based on the respective random rate of EVR-like, α-like, escape-like, and SF-like events in that pixel. These values were summed across the entire detector and across all files to obtain the true number of expected random decay chains. For ^{288}Fl, we calculate that the number of expected random chains generated from background events that meet the search conditions defined in Sec. III A is 2.2×10^{-6} random ^{288}Fl EVR-α-SF correlations or 1.8×10^{-3} random ^{288}Fl

EVR-esc-SF correlations. The number of expected EVR-α−α-SF random chains generated from background events that meet the search conditions defined for ^{289}Fl is 6.6×10^{-5} across the entire experiment.

H. Random correlations

As discussed in Sec. III A, correlation search conditions for the experiment were broad to enable a more complete understanding of background in the detector. In addition to the searches described above in Sec. III A, we also investigated potential correlations between

(1) EVR [$11 \leqslant E$(MeV) $\leqslant 30$] or TRP [$30 \leqslant E$(MeV) $\leqslant 100$] followed by an α-like event [$6 \leqslant E$(MeV) $\leqslant 12$] within 1000 s;
(2) EVR or TRP followed by at least two α-like events with each α having a correlation time of $\leqslant$1000 s;
(3) EVR or TRP followed by an SF-like event [$E \geqslant 60$ MeV] within 1000 s;
(4) EVR followed by one or more α-like events followed by an SF-like event with all decays having correlation times $\leqslant$1000 s;
(5) combinations of the above correlations with escape-like [E(MeV) $\leqslant 5$] events in place of one or more α-like events;
(6) search backward from each SF-like event with $E \geqslant 120$ MeV for potential EVR or α-like events within 1000 s;
(7) correlations between an α-like event followed by an SF-like event within 1000 s, where it is assumed that the EVR was missing.

1. EVR-α and EVR-SF

All observed correlations between an EVR-like event and an α-like event that follows within 1000 s are shown in Fig. 8(b). Random correlations between unrelated EVRs and α-like events begin to occur around 0.1 s and dominate the random background by correlation times of ≈10 s. However, we do not observe significant background from α decays of short-lived transfer reaction products that contribute significantly to the background in other separators [55]. This is due to the larger bend angle of the BGS ($25^\circ + 45^\circ = 70^\circ$) when compared with other gas-filled separators that tend to have bending angles in the range of about $20^\circ - 35^\circ$. The larger bend angle increases the separation between the EVRs of SHE and recoiling TRP, reducing the background at the position of the SHREC detector.

The same data are shown for EVR-SF correlations in Fig. 8(a). At lower SF energies, $E_{SF} \leqslant 120$ MeV, where background is higher, random EVR-SF correlations begin to appear at around 1 s. This rate decreases quickly as the SF energy increases. At SF energies $E_{SF} \geqslant 120$ MeV, which correspond to energies expected for SF decays from Fl descendants, there are significantly fewer correlations in Fig. 8(a). They form a cluster in the range 0.1−10 s. This behavior is clearly different from the lower-energy SF-like events. Based on this behavior and the high-energy spectra shown in Fig. 6(b), possible SF events originating from the decay of $^{287-289}$Fl or its daughters were required to have energies greater than 120 MeV.

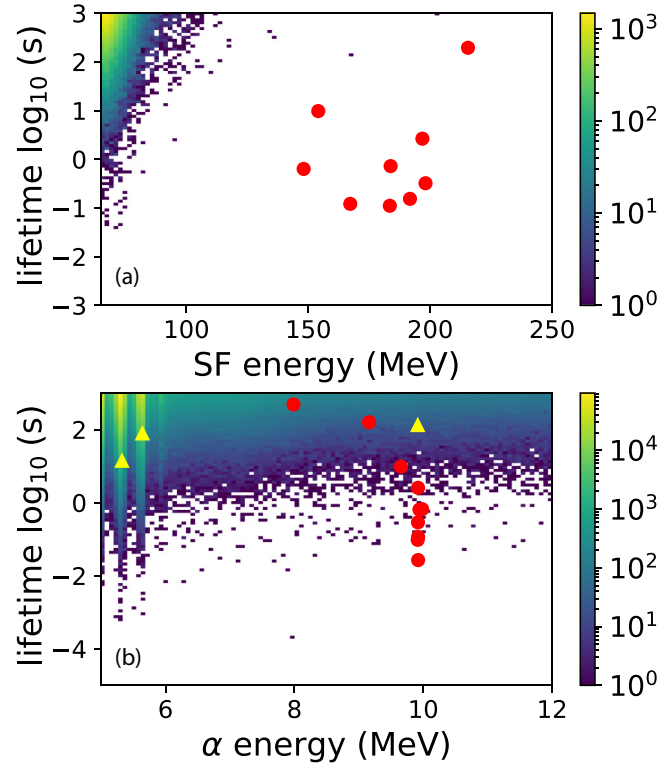

FIG. 8. Panel (a) shows all observed EVR-SF (unfilled, blue circles) and EVR-SF correlations assigned to the decay of $^{287-289}$Fl (solid, red circles). Panel (b) shows EVR-α correlations (unfilled, blue circles) and all EVR-α correlations followed by an SF-like event in the same pixel within 1000 s of the α assigned in decay of $^{287-289}$Fl (solid, red circles) and to random correlations (solid, yellow triangles). The color bars indicate the total number of correlations observed per pixel over the entire experiment.

Based on the rate of EVR-like events, we expect 3.6 random correlations between EVR-like and SF-like events with $E_{SF} \geqslant 120$ MeV. In the data, a total of 13 EVR-SF correlations were observed. Nine were correlations comprising the EVR and SF events from chains 1–9 in Table II. There were four additional EVR-SF correlations that were not assigned to decay chains of Fl isotopes. These are shown in Table V. An additional search was performed for these potential chains, looking for α particles that the online search may have missed, escaping α particles that deposit only a fraction of their energy

TABLE V. EVR-SF correlations with SF correlation times <1000 s that were not assigned to a decay chain of $^{287-289}$Fl.

Chain ID	x strip	y strip	E_{EVR} (MeV)	E_{SF} (MeV)	Correlation Time (s)
a	4	34	24.8	137	304
b	135	7	15.8	168	133
c	1	41	12.8	202	978
d	98	48	26.0	134	390

in the implantation detector, and upstream-only events where the escaping α particle deposited an energy in the implantation detector that could have been below the energy threshold to trigger the relevant channel of the data acquisition. For three of the chains (labeled "a," "c," and "d" in Table V), no other potential decay chain members were identified. Based on the long correlation times between the events in those chains and the number of expected random correlations, they were assigned to random correlations of unrelated events. In chain "b," there was an additional EVR in the same pixel 132.7 s after the EVR listed for chain b in Table V. The second EVR was followed 121 ms later by a 9.91-MeV α particle, and terminated 26 ms later by the SF event. This second EVR-α-SF correlation was assigned to ^{288}Fl and corresponds to chain 1 in Table II. The 15.8-MeV EVR and the preceding SF in chain b of Table V were thus assigned as a random correlation to a true ^{288}Fl SF decay.

Only ten EVR-α-SF correlations were observed where the SF energy was $E_{\mathrm{SF}} \geqslant 120$ MeV and the α energy was $E_\alpha >$ 8 MeV. Nine of these were assigned to the decay of $^{287-289}$Fl as discussed in Secs. III C–III E. They are listed as chains 1–9 in Table II. The tenth correlation was the additional random EVR that was correlated to chain 1 as described above. The α-particle-energy window was then widened to include all α-like events with $5 \leqslant E_\alpha(\mathrm{MeV}) \leqslant 11$. Only two more EVR-$\alpha$-SF correlations were observed. The α correlation times and energies are shown by the yellow triangles in Fig. 8. The observed α energies for those correlations were consistent with α-particle energies from the calibration source that randomly correlated to EVR and SF-like events over the 1000 s correlation window. In experiments at other gas-filled separators, a common source of short-lived EVR-SF background is from actinide isomers that are formed in transfer reactions between the beam and the target. No such isomers were observed in this work, and this is consistent with other experiments with actinide targets at the BGS [40,45,82,83].

2. TRP-α and TRP-SF

All observed correlations between TRP-like events and SF-like events are shown in Fig. 9(a). As was previously seen with EVR-SF correlations, random correlations between lower-energy SF-like events ($E_{\mathrm{SF}} \leqslant 120$ MeV) and TRP begin to occur already around 0.1 s. As the SF energy threshold is increased, the number of potential SF-like events decreases, corresponding to a decreasing rate of random TRP-SF correlations. Based on the random rates from Sec. III G, we would expect to observe about 11 random TRP-SF correlations with $E_{\mathrm{SF}} \geqslant 120$ MeV, while 50 such events are observed. Five of these events can be attributed to TRP-like events randomly correlating to SF events from the identified Fl decay chains. However, that still indicates that about four times as many TRP-SF events were observed than expected through random correlations. A full discussion of this type of TRP events observed during SHE experiments at the BGS is the subject of a forthcoming presentation.

All observed correlations between TRP-like and α-like events are displayed in Fig. 9(b). Our data indicate that these random correlations begin to occur around 0.1 s. Similar to the EVR-α correlations, there are no distinct peaks in the correlation plot that can be attributed to the detection of a significant number of α decays originating from near-target-like TRPs.

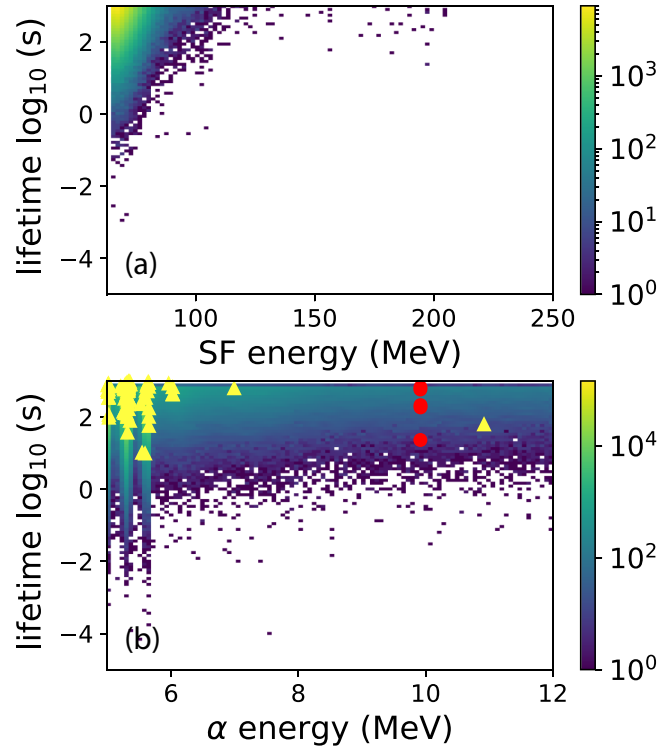

FIG. 9. Panel (a) shows all observed TRP-SF correlations with correlation times $\leqslant$1000 s. Panel (b) shows TRP-α correlations with $30 \leqslant E_{\mathrm{TRP}}(\mathrm{MeV}) \leqslant 70$ and correlation times between the TRP and $\alpha \leqslant 1000$ s (blue circles) as well as all TRP-α correlations followed by an SF-like event in the same pixel within 1000 s of the α assigned in decay of $^{287-289}$Fl (solid red circles) and to random correlations (solid yellow triangles), respectively. The color bars indicate the total number of correlations observed per pixel over the entire experiment.

Searching for TRP-α-SF correlations while considering only SF-like events with $E_{\mathrm{SF}} \geqslant 120$ MeV, 83 TRP-α-SF correlations are observed. Seventy-six of these can be attributed to random correlations with the α calibration source or the ^{242}Cm activity (see Sec. II). An additional five are attributed to random TRP correlating to identified Fl decay chains, where the TRP preceded the EVR by tens of seconds. The other two correlations are detailed in Table VI. We expect to observe 1.3 random TRP-α-SF events with the energy and correlation time search windows of this analysis, and therefore these events are attributed to random correlations.

I. Systematic error

Systematic uncertainties on the cross sections measured at the BGS have been discussed previously in Ref. [85] but are recapped briefly here. It is estimated that systematic uncertainties result from five main contributions discussed here. The first is the uncertainty in the efficiency for transporting EVRs to the SHREC detector. This error was estimated by sending EVRs of ^{254}No from the ^{208}Pb(^{48}Ca, $2n$) reaction through the

TABLE VI. TRP-α-SF correlations with SF correlation times <1000 s, where the α-SF correlation was not assigned to a decay chain of $^{287-289}$Fl.

Chain ID	x strip	y strip	E_{TRP} (MeV)	E_α (MeV)	Correlation Time (s)	E_{SF} (MeV)	Correlation Time (s)
e	87	21	39.5	6.99(2)	628	154	530
f	17	6	49.1	10.9(1)	62.8	121	780

BGS and comparing the size and shape of the ^{254}No implantation distribution on the focal plane detector to distributions that were modeled using the simulation code described in Ref. [61]. Based on this comparison, it is estimated that the error on the EVR collection efficiency is $\sigma_{\text{eff}}/\text{eff} = 10\%$. The second is the uncertainty in the angle of the Rutherford detectors is 0.1° with respect to the beam axis. For the beam used in this experiment, this results in a 3% uncertainty in the Rutherford cross section and a corresponding 3% uncertainty in the calculated EVR cross section. A third contribution is due to the fact that upstream of each Rutherford detector is a collimator that reduces the number of scattered particles impacting the detectors. The uncertainty in the size of this collimator is the main contribution to uncertainty in the angle subtended by this collimator and is estimated to contribute 4% to the systematic error in the cross sections. Two attenuation screens are situated between the target and the Rutherford detectors to reduce the intensity of Rutherford-scattered particle impacting the detectors, and introduce a fourth source of uncertainty. The attenuation factor of these screens was measured using the ^{207}Pb(^{48}Ca, $2n$) reaction. EVRs of ^{253}No were sent to the focal plane detector with and without the attenuation screens in place, and the ratio of ^{253}No EVRs to Rutherford-scattered particles was measured [86]. It is estimated that the uncertainty in the attenuation factor contributes 5% to the systematic error. The last contribution to the systematic uncertainty comes from the uncertainty in the absolute energy from the 88-Inch Cyclotron, which is estimated to be 1%. While the beam energy was measured to a higher precision than that for this experiment, that measurement was performed on a neighboring beamline. It is not certain that the same turn out of the cyclotron, and therefore the same beam energy, is extracted for both beamlines. Therefore, that value is used as a measurement of relative change in beam energy between different tunes. Error propagation of the five sources of uncertainty indicates that the systematic error on cross sections reported at the BGS are 12%.

IV. CONCLUSION

The SHREC detector equipped with digital electronics [62] was installed at the BGS focal plane and, together with other facility improvements, commissioned into the SHE regime of the nuclidic chart using the ^{244}Pu(^{48}Ca, xn)$^{292-x}$Fl reaction. Seven decay chains were observed and assigned to the $4n$ exit channel, ^{288}Fl. The observed cross section for this experiment of 6.7 $(^{36}_{25})$pb is consistent with previously published values. Our observed α-particle energies also strongly agree with those previously published from Ref. [46] and demonstrate the high-resolution capabilities of the new system. The decay characteristics of all hitherto reported decay chains starting from or passing through ^{288}Fl are updated. Furthermore, one decay chain of ^{287}Fl and one decay chain ^{289}Fl were identified in this experiment. Another chain was tentatively identified as originating from ^{289}Fl. The decay properties observed, as well as the performance of SHREC and the new electronics, are extensively discussed. The results from this commissioning experiment demonstrate that, after combining the highly efficient BGS with the SHREC detector and new digital electronics, LBNL is well-positioned to investigate the properties of SHEs with higher precision than ever before.

ACKNOWLEDGMENTS

We gratefully acknowledge the operations staff of the 88-Inch Cyclotron for providing the intense beams of ^{50}Ti and stable operating conditions. This work was supported in part by the U.S. Department of Energy, Office of Science, Office of Nuclear Physics under Contracts No. DE-AC02-05CH11231 (LBNL) and No. DE-FG02-93ER40773 (TAMU); U.S. Department of Energy, Office of Science, Office of Basic Energy Sciences under Contract No. DE-AC02-05CH11231 (LBNL); the Swedish Knut and Alice Wallenberg Foundation (Grant No. KAW 2015.0021), the Wenner-Gren Foundations (Grant No. SSv2020-0003), the Carl Trygger Foundation (CTS 20:1146), and the Royal Physiographic Society in Lund; startup package from the Oregon State University College of Engineering (OSU); and the U.S. Department of Energy under Contract No. DE-AC52-07NA27344 (LLNL). The authors are indebted (for the use of ^{244}Pu) to the U.S. Department of Energy, through the transplutonium element production facilities at Oak Ridge National Laboratory.

DATA AVAILABILITY

The data that support the findings of this article are under embargo until December 31, 2026. After this time, they will be available from the authors upon reasonable request.

[1] S. Hofmann, S. N. Dmitriev, C. Fahlander, J. M. Gates, J. B. Roberto, and H. Sakai, On the discovery of new elements (IUPAC/IUPAP report), Pure Appl. Chem. **92**, 1387 (2020).

[2] C. Perrier and E. Segrè, Some chemical properties of element 43, J. Chem. Phys. **5**, 712 (1937).

[3] Y. T. Oganessian, A. Sobiczewski, and G. M. Ter-Akopian, Superheavy nuclei: From predictions to discovery, Phys. Scr. **92**, 023003 (2017).

[4] S. Hofmann, Super-heavy nuclei, J. Phys. G **42**, 114001 (2015).

[5] S. Hofmann, *et al.*, The new element 112, Z. Phys. A: Hadrons Nucl. **354**, 229 (1996).

[6] Special issue on superheavy elements, Nucl. Phys. A **944** (2015).

[7] L. Öhrström and J. Reedijk, Names and symbols of the elements with atomic numbers 113, 115, 117 and 118 (IUPAC recommendations 2016), Pure Appl. Chem. **88**, 1225 (2016).

[8] K. Morita, *et al.*, Experiment on the synthesis of element 113 in the reaction ^{209}Bi(^{70}Zn, n)^{278}113, J. Phys. Soc. Jpn. **73**, 2593 (2004).

[9] K. Morita, *et al.*, New result in the production and decay of an isotope, ^{278}113, of the 113th element, J. Phys. Soc. Jpn. **81**, 103201 (2012).

[10] Y. T. Oganessian, *et al.*, Synthesis of the isotope ^{282}113 in the ^{237}Np + ^{48}Ca fusion reaction, Phys. Rev. C **76**, 011601(R) (2007).

[11] O. R. Smits, Ch. E. Düllmann, P. Indelicato, W. Nazarewicz, and P. Schwerdtfeger, The quest for superheavy elements and the limit of the periodic table, Nat. Rev. Phys. **6**, 86 (2024).

[12] G. Scharff-Goldhaber, Nucleonics **15**, 122 (1957).

[13] W. D. Myers and W. J. Swiatecki, Nuclear masses and deformations, Nucl. Phys. **81**, 1 (1966).

[14] A. Sobiczewski, F. A. Gareev, and B. N. Kalinkin, Closed shells for $Z > 82$ and $N > 126$ in a diffuse potential well, Phys. Lett. **22**, 500 (1966).

[15] S. G. Nilsson, C. F. Tsang, A. Sobiczewski, Z. Szymański, S. Wycech, C. Gustafson, I.-L. Lamm, P. Möller, and B. Nilsson, On the nuclear structure and stability of heavy and superheavy elements, Nucl. Phys. A **131**, 1 (1969).

[16] S. Ćwiok, J. Dobaczewski, P.-H. Heenen, P. Magierski, and W. Nazarewicz, Shell structure of the superheavy elements, Nucl. Phys. A **611**, 211 (1996).

[17] V. Zagrebaev and W. Greiner, Synthesis of superheavy nuclei: A search for new production reactions, Phys. Rev. C **78**, 034610 (2008).

[18] G. G. Adamian, N. V. Antonenko, and W. Scheid, Feature of production of new superheavy nuclei in actinide-based complete-fusion reactions, Eur. Phys. J. A **41**, 235 (2009).

[19] A. K. Nasirov, G. Mandaglio, G. Giardina, A. Sobiczewski, and A. I. Muminov, Effects of the entrance channel and fission barrier in the synthesis of superheavy element $Z = 120$, Phys. Rev. C **84**, 044612 (2011).

[20] N. Wang, J. Tian, and W. Scheid, Systematics of fusion probability in "hot" fusion reactions, Phys. Rev. C **84**, 061601(R) (2011).

[21] Z.-H. Liu and J.-D. Bao, Role of the coupling between neck and radial degrees of freedom in evolution from dinucleus to mononucleus, Phys. Rev. C **83**, 044613 (2011).

[22] K. Siwek-Wilczyńska, T. Cap, M. Kowal, A. Sobiczewski, and J. Wilczyński, Predictions of the fusion-by-diffusion model for the synthesis cross sections of $Z = 114-120$ elements based on macroscopic-microscopic fission barriers, Phys. Rev. C **86**, 014611 (2012).

[23] N. Wang, E.-G. Zhao, W. Scheid, and S.-G. Zhou, Theoretical study of the synthesis of superheavy nuclei with $Z = 119$ and 120 in heavy-ion reactions with trans-uranium targets, Phys. Rev. C **85**, 041601(R) (2012).

[24] A. N. Kuzmina, G. G. Adamian, N. V. Antonenko, and W. Scheid, Influence of proton shell closure on production and identification of new superheavy nuclei, Phys. Rev. C **85**, 014319 (2012).

[25] Z.-H. Liu and J.-D. Bao, Possibility to produce element 120 in the ^{54}Cr + ^{248}Cm hot fusion reaction, Phys. Rev. C **87**, 034616 (2013).

[26] J. Jiang, Q. Chai, B. Wang, W. Zhao, M. Liu, and H. Wang, Investigation of production cross sections for superheavy nuclei with $Z = 116$–121 in dinuclear system concept, Nucl. Phys. Rev. **30**, 4 (2013).

[27] J. Zhang, C. Wang, and Z. Ren, Calculation of evaporation residue cross sections for the synthesis of superheavy nuclei in hot fusion reactions, Nucl. Phys. A **909**, 36 (2013).

[28] L. Zhu, W.-J. Xie, and F.-S. Zhang, Production cross sections of superheavy elements $Z = 119$ and 120 in hot fusion reactions, Phys. Rev. C **89**, 024615 (2014).

[29] V. I. Zagrebaev and W. Greiner, Cross sections for the production of superheavy nuclei, Nucl. Phys. A **944**, 257 (2015).

[30] G. G. Adamian, N. V. Antonenko, H. Lenske, and L. A. Malov, Predictions of identification and production of new superheavy nuclei with $Z = 119$ and 120, Phys. Rev. C **101**, 034301 (2020).

[31] F. Niu, P. Chen, and Z. Feng, Systematics on production of superheavy nuclei $Z = 119-122$ in fusion-evaporation reactions, Nucl. Sci. Tech. **32**, 103 (2021).

[32] J.-X. Li and H.-F. Zhang, Predictions for the synthesis of the $Z = 119$ superheavy element, Phys. Rev. C **105**, 054606 (2022).

[33] J.-X. Li and H.-F. Zhang, Predictions for the synthesis of the $Z = 120$ superheavy element, Phys. Rev. C **106**, 034613 (2022).

[34] S. H. Zhu and X. J. Bao, Possibility to synthesize $Z = 120$ superheavy nuclei with $Z > 20$ projectiles, Phys. Rev. C **108**, 014604 (2023).

[35] J.-J. Li, N. Tang, Y.-H. Zhang, M.-H. Zhang, C. Wang, X.-R. Zhang, L. Zhu, and F.-S. Zhang, Progress on production cross-sections of unknown nuclei in fusion evaporation reactions and multinucleon transfer reactions, Int. J. Mod. Phys. E **32**, 2330002 (2023).

[36] S. Hofmann, *et al.*, Probing shell effects at $Z = 120$ and $N = 184$, Technical Report No. NUSTAR-SHE-01 (GSI Scientific Report, 2008), https://repository.gsi.de/record/53523.

[37] Y. T. Oganessian, *et al.*, Attempt to produce element 120 in the ^{244}Pu + ^{58}Fe reaction, Phys. Rev. C **79**, 024603 (2009).

[38] J. Khuyagbaatar, *et al.*, Search for elements 119 and 120, Phys. Rev. C **102**, 064602 (2020).

[39] S. Hofmann, *et al.*, New results on elements 111 and 112, Eur. Phys. J. A **14**, 147 (2002).

[40] J. M. Gates, *et al.*, Toward the discovery of new elements: Production of livermorium ($Z = 116$) with ^{50}Ti, Phys. Rev. Lett. **133**, 172502 (2024).

[41] Y. T. Oganessian, From past to future in the science of super heavy elements, Eur. Phys. J. A **60**, 227 (2024).

[42] P. Möller, J. Nix, and K.-L. Kratz, Nuclear properties for astrophysical and radioactive-ion-beam applications, At. Data Nucl. Data Tables **66**, 131 (1997).

[43] A. Sobiczewski, Predictions for a superheavy element 120, Acta Phys. Pol. B **42**, 1871 (2011).

[44] D. Rudolph, *et al.*, Spectroscopy of element 115 decay chains, Phys. Rev. Lett. **111**, 112502 (2013).

[45] J. M. Gates, *et al.*, Decay spectroscopy of element 115 daughters: ^{280}Rg → ^{276}Mt and ^{276}Mt → ^{272}Bh, Phys. Rev. C **92**, 021301(R) (2015).

[46] A. Såmark-Roth, Spectroscopy along flerovium decay chains: Discovery of ^{280}Ds and an excited state in ^{282}Cn, Phys. Rev. Lett. **126**, 032503 (2021).

[47] D. M. Cox, *et al.*, Spectroscopy along flerovium decay chains. II. Fine structure in odd-A ^{289}Fl, Phys. Rev. C **107**, L021301 (2023).

[48] A. Såmark-Roth, Spectroscopy along flerovium decay chains: III. Details on experiment, analysis, ^{282}Cn, and spontaneous fission branches, Phys. Rev. C **107**, 024301 (2023).

[49] J. L. Pore, *et al.*, Spontaneous fission of the odd-Z isotope ^{255}Db, Phys. Rev. C **110**, L041301 (2024).

[50] J. Khuyagbaatar, *et al.*, Stepping into the sea of instability: The new sub-μs superheavy nucleus ^{252}Rf, Phys. Rev. Lett. **134**, 022501 (2025).

[51] J. M. Gates and J. L. Pore, Studies of heavy and super heavy elements with FIONA: The broad impact of mass-number identifications, Eur. Phys. J. A **58**, 196 (2022).

[52] Y. T. Oganessian, *et al.*, Synthesis of superheavy nuclei in the ^{48}Ca + ^{244}Pu reaction: ^{288}114, Phys. Rev. C **62**, 041604(R) (2000).

[53] Y. T. Oganessian, *et al.*, Measurements of cross sections for the fusion-evaporation reactions ^{244}Pu (^{48}Ca, xn)$^{292-x}$114 and ^{245}Cm (^{48}Ca, xn)$^{293-x}$116, Phys. Rev. C **69**, 054607 (2004).

[54] Ch. E. Düllmann, *et al.*, Production and decay of element 114: High cross sections and the new nucleus ^{277}Hs, Phys. Rev. Lett. **104**, 252701 (2010).

[55] J. M. Gates, *et al.*, First superheavy element experiments at the GSI recoil separator TASCA: The production and decay of element 114 in the ^{244}Pu(^{48}Ca, 3−4n) reaction, Phys. Rev. C **83**, 054618 (2011).

[56] D. Leitner, S. R. Abbott, R. D. Dwinell, M. Leitner, C. Taylor, and C. M. Lyneis, Commissioning of the superconducting ECR ion source VENUS, in *Proceedings of the 2003 Particle Accelerator Conference, Portland, OR* (IEEE, Piscataway, NJ, 2003), Vol. 1, p. 86.

[57] D. Leitner, C. M. Lyneis, S. R. Abbott, D. Collins, R. D. Dwinell, M. L. Galloway, M. Leitner, and D. S. Todd, Next generation ECR ion sources: First results of the superconducting 28 GHz ECRIS – VENUS, Nucl. Instrum. Methods Phys. Res. Sect. B **235**, 486 (2005).

[58] M. Kireeff Covo, Nondestructive synchronous beam current monitor, Rev. Sci. Instrum. **85**, 125106 (2014).

[59] J. F. Ziegler, SRIM-2003, Nucl. Instrum. Methods Phys. Res. Sect. B **219-220**, 1027 (2004).

[60] W. D. Myers and W. J. Swiatecki, Nuclear properties according to the Thomas-Fermi model, Nucl. Phys. A **601**, 141 (1996).

[61] K. E. Gregorich, Simulation of recoil trajectories in gas-filled magnetic separators, Nucl. Instrum. Methods Phys. Res., Sect. A **711**, 47 (2013).

[62] P. Golubev, *et al.*, Source characterization of a detector for heavy and superheavy nuclei, Nucl. Instrum. Methods Phys. Res., Sect. A **1075**, 170384 (2025).

[63] P. Golubev, *et al.*, The Lund–York–Cologne Calorimeter (LYCCA): Concept, design and prototype developments for a FAIR-NUSTAR detector system to discriminate relativistic heavy-ion reaction products, Nucl. Instrum. Methods Phys. Res. Sect. A **723**, 55 (2013).

[64] See CAEN CoMPASS documentation at https://www.caen.it/products/compass/ (Access: May, 2024).

[65] Y. T. Oganessian, *et al.*, Observation of the decay of ^{292}116, Phys. Rev. C **63**, 011301(R) (2000).

[66] Y. T. Oganessian, V. K. Utyonkov, and K. J. Moody, Synthesis of ^{292}116 in the ^{248}Cm + ^{48}Ca reaction, Phys. At. Nucl. **64**, 1349 (2001).

[67] Y. T. Oganessian, *et al.*, Heavy element research at Dubna, Nucl. Phys. A **734**, 109 (2004).

[68] A. Yakushev, *et al.*, Superheavy element flerovium (element 114) is a volatile metal, Inorg. Chem. (Washington, DC, US) **53**, 1624 (2014).

[69] A. Yakushev, *et al.*, On the adsorption and reactivity of element 114, flerovium, Front. Chem. (Lausanne, Switzerland) **10**, 976635 (2022).

[70] S. Hofmann, *et al.*, The reaction ^{48}Ca + ^{248}Cm →^{296} 116* studied at the GSI-SHIP, Eur. Phys. J. A **48**, 62 (2012).

[71] D. Kaji, *et al.*, Study of the reaction ^{48}Ca + ^{248}Cm → ^{296}Lv ∗ at RIKEN − GARIS, J. Phys. Soc. Jpn. **86**, 034201 (2017).

[74] See Supplemental Material at http://link.aps.org/supplemental/10.1103/kjyy-t1nk for detailed results and statistical assessment of decay chain members originating from the isotope ^{287}Fl.

[75] Y. T. Oganessian, *et al.*, Investigation of ^{48}Ca-induced reactions with ^{242}Pu and ^{238}U targets at the JINR superheavy element factory, Phys. Rev. C **106**, 024612 (2022).

[74] Y. T. Oganessian, *et al.*, Synthesis of the isotopes of elements 118 and 116 in the ^{249}Cf and ^{245}Cm + ^{48}Ca fusion reactions, Phys. Rev. C **74**, 044602 (2006).

[75] S. Hofmann, *et al.* Review of even element super-heavy nuclei and search for element 120, Eur. Phys. J. A **52**, 180 (2016).

[76] F. Heßberger, Nuclear structure of the transactinides – investigated by decay spectroscopy, EPJ Web Conf. **131**, 02005 (2016).

[77] D. Rudolph, Results and plans for nuclear spectroscopy of superheavy nuclei: The Lund perspective, Eur. Phys. J. A **58**, 242 (2022).

[78] C. Qi, F. R. Xu, R. J. Liotta, R. Wyss, M. Y. Zhang, C. Asawatangtrakuldee, and D. Hu, Microscopic mechanism of charged-particle radioactivity and generalization of the Geiger-Nuttall law, Phys. Rev. C **80**, 044326 (2009).

[79] K.-H. Schmidt, A new test for random events of an exponential distribution, Eur. Phys. J. A **8**, 141 (2000).

[80] Y. T. Oganessian, *et al.*, Measurements of cross sections and decay properties of the isotopes of elements 112, 114, and 116 produced in the fusion reactions ^{233,238}U, ^{242}Pu, and ^{248}Cm + ^{48}Ca, Phys. Rev. C **70**, 064609 (2004).

[81] S. Hofmann, D. Ackermann, and S. Antalic, *et al.*, The reaction ^{48}Ca + ^{238}U →^{286} 112* studied at the GSI-SHIP, Eur. Phys. J. A **32**, 251 (2007).

[82] L. Stavsetra, K. E. Gregorich, J. Dvorak, P. A. Ellison, I. Dragojević, M. A. Garcia, and H. Nitsche, Independent verification of element 114 production in the ^{48}Ca + ^{242}Pu reaction, Phys. Rev. Lett. **103**, 132502 (2009).

[83] P. A. Ellison, *et al.*, New superheavy element isotopes: ^{242}Pu(^{48}Ca, 5n) ^{285}114, Phys. Rev. Lett. **105**, 182701 (2010).

[84] Y. T. Oganessian, *et al.*, Synthesis and decay properties of isotopes of element 110: ^{273}Ds and ^{275}Ds, Phys. Rev. C **109**, 054307 (2024).

[85] K. E. Gregorich, *et al.*, Attempt to confirm superheavy element production in the ^{48}Ca + ^{238}U reaction, Phys. Rev. C **72**, 014605 (2005).

[86] C. M. Folden III, Development of odd-Z-projectile reactions for transactinide element synthesis, Ph.D. thesis, University of California, Berkeley, 2004.